Combined ab Initio Quantum Mechanics and Classical Molecular Dynamics Studies of Polyphosphazene Polymer Electrolytes: Competitive Solvation of Li^+ and $LiCF_3SO_3$

Yixuan Wang* and Perla B. Balbuena*

Department of Chemical Engineering, Texas A&M University, College Station, Texas 77843

Received: May 22, 2004; In Final Form: July 30, 2004

Ab initio quantum mechanics (QM) and classical molecular dynamics (MD) simulations are employed to model an electrolyte composed of a polyphosphazene (PP), lithium triflate ($LiCF_3SO_3$), and water. Structures and energetics are systematically studied by QM for binary complexes of Li^+, $CF_3SO_3^-$, and $Li^+CF_3SO_3^-$ with water or PP fragments, and for ternary combinations of $Li^+CF_3SO_3^-$, PP fragments, and water. Li^+ interacts most strongly with the backbone nitrogen of PP, somewhat more weakly (and comparably) with ether oxygens on PP side chains and with water oxygens. This indicates that Li^+−N interactions should significantly affect migration of Li^+ in PP polymer electrolytes. Calculated coordination patterns of Li^+ with the poly(ethylene oxide) model (ethylene oxide)$_6$ [$(EO)_6$] agree with experimental results in which Li^+ is strongly coordinated with five oxygens in PEO. Binary aggregates of $LiCF_3SO_3$ and $(EO)_6$ are also examined. Both Li^+ and $LiCF_3SO_3$ coordinate preferentially with neighboring N atoms and a methoxy oxygen near the PP backbone. Classical MD simulations qualitatively reproduce the results of QM calculations, and provide details about the Li^+ distribution in a larger system. Results of the QM and classical MD calculations suggest a model for the microstructure of the polyelectrolyte.

1. Introduction

Polyphosphazene (PP) polymers, such as poly[bis(2-(2′-methoxyethoxy)ethoxy)phosphazene] (MEEP, $(-P(OCH_2CH_2OCH_2CH_2OCH_3)_2{=}N-)_n$) have been proposed as potential polymer electrolytes for lithium batteries,[1] because their room temperature ionic conductivity when "salted" can be 1−3 orders of magnitude higher than that of earlier ionically conductive salted polymers based on poly(ethylene oxide) (PEO).[2] Although the conductivity of MEEP is still far from the value generally thought to be required for moderate-rate power sources (10^{-3} S/cm at room temperature), combinations of salted PP solid polymers and small amounts of liquid additive (forming gel PP polymer electrolytes) open a door to raising ionic conductivity to useful values. Alternatively, structural modifications of PPs might also improve their ionic conductivity. Much research has been devoted to synthesizing novel PPs and characterizing new and existing PPs.[1,3] PPs like other polymer electrolytes are also anion conductors.

In Li/sea water batteries,[4] a potentially attractive marine power source, PP-based electrolytes might be used as protective membranes, attached as thin films to the lithium anode.[5] These membranes would need to be highly hydrophobic, to prevent parasitic reaction of water with the lithium anode, yet be sufficiently ionically conductive to allow Li^+ transport at required rates. Additionally, the membrane would need to adhere strongly to the anode (lithium) surface, maintaining intimate contact between the membrane and the metal as the substrate is oxidized to form Li^+ ions and those ions enter and diffuse through the polymer layer. Li^+ is expected to have very complex interactions with the involved species in the membrane. For instance, Li^+ can be solvated by the Lewis base groups of PP, such as ether oxygens in the side chains, and backbone N atoms. Li^+ should also interact with water molecules coming through the PP membrane from the cathode side. In fact, permeation of water into the membrane may help to dissolve the lithium salts, possibly increasing ionic conductivity as a similar phenomenon does in gel polymer electrolytes. Another important set of interactions occurs between Li^+ and anions, particularly the electrolyte salt anion (and, if they diffuse into the membrane, other anions ubiquitous in sea water, e.g., Cl^-, HCO_3^-, and OH^-). All of these interactions can affect the behavior of PP-based electrolytes as anode protective membranes for Li/sea water batteries; they can also strongly affect ionic transport mechanisms in PP matrixes. Specifically, the relative strength of these interactions influences the relative importance of Li^+ (as opposed to anion) migration in ionic conductivity, and the nature of solvated species in active PP electrolytes. Detailed knowledge of primary solvation structures is necessary to predict the transport properties needed for mathematical modeling of water permeation through a membrane to the Li metal surface.

Since the discovery of ionic conduction in PEO,[2] the interactions of Li^+ with the PEO matrix and its additives in PEO-based gels have been intensively studied, by experimental and theoretical means, with the aim of understanding ionic transport in that medium.[6−10] Plausible and widely accepted mechanisms for lithium ion transport in PEO membranes include hopping of lithium cations between neighboring PEO molecules and between contiguous sets of ether oxygens along individual polymer molecules.[3,4] Recently, the mechanism of Li^+ cation transport through PP electrolytes has been addressed, but the conclusions are considerably more controversial. For example, Luther et al. concluded that the preferred association of Li^+ cation with the PP polymer MEEP is via both backbone nitrogen and neighboring oxygens (in the side groups), forming pocket-like conformations along the backbone.[11] This conclusion is

* Address correspondence to the authors at e-mail yixuan.wang@chemail.tamu.edu and balbuena@tamu.edu.

10.1021/jp047782t CCC: $27.50
Published on Web 09/11/2004

different than the one previously reached by Allcock,[12] who concluded that interaction of Li^+ with backbone nitrogens was not important in ionic conduction in PP gels (composed of PP, salt, and DMF).

In this paper, we model ternary PP-based electrolytes, consisting of lithium triflate ($LiCF_3SO_3$), (model) PPs, and water. Our objectives are to determine (1) the most favorable conformation of the PP backbone, (2) comparative energies of solvation of Li^+ by other active species, and (3) geometries of Li^+ solvation structures near ether-containing side groups and the backbone of PPs. Some relevant species have been previously investigated by ab initio molecular orbital theory, including the $Li^+-CF_3SO_3^-$ contact ion pair (CIP),[13] Li^+-H_2O,[14] and Li^+-ether oxygen in $(CH_2CH_2O)_m$ complexes.[9,10,15,34,35] For the sake of self-consistency, particularly with respect to necessary corrections, like zero point energy (ZPE) and basis set superposition error (BSSE) corrections, we did our own calculations for these systems. Cation−water and cation−model polymer interactions were examined with ab initio molecular orbital theory (HF/6-31G*) and/or density functional theory (B3PW91/6-31G*). Keeping in mind the debate about the interaction of Li^+ with the backbone nitrogen of PPs, attention was paid to the backbone structure and to the interactions of Li^+ with the backbone nitrogen. Binary CIP−model polymer as well as ternary H_2O-CIP−model polymer complexes were also examined. The results allow us to suggest likely candidates for the primary solvation structures in PP-based electrolytes. Classical molecular dynamics (MD) are used to confirm conclusions obtained from the ab initio calculations in larger model systems. The calculations suggest a preferred Li^+ distribution in PP polymer-based gel electrolytes.

2. Computational Details

2.1. Ab Initio Quantum Chemistry Calculations. The equilibrium structures of all the involved species were fully optimized by ab initio molecular orbital theory HF/6-31G* and/or B3PW91/6-31G* hybrid generalized gradient approximation density functional theory.[16,17] Single-point calculations were also used for some small and medium systems at a higher level: B3PW91/6-311++G(p,d) energy calculations for HF/6-31G* optimized structures, designated as B3PW91/6-311++G(d,p)//HF/6-31G* results below. To characterize the stationary points and make the zero point energy (ZPE) corrections, a frequency analysis was done for most of the systems, using the same methods employed for the geometry optimization. If not noted otherwise, relative energies refer to values with ZPE correction; enthalpies and Gibbs free energies are calculated at 298.2 K. Atomic charges are calculated by fitting the molecular electrostatic potential (CHelpG method).[18] Basis set superposition error (BSSE) corrections[19] are estimated for some complexes.

To estimate solvent effects beyond those provided by cluster models, the conductor-like polarizable continuum model (CPCM)[20,21] is employed in single-point calculations. In CPCM, the variation of the free energy when going from vacuum to solution consists of the work required to build a cavity in the solvent (cavitation energy), plus electrostatic and nonelectrostatic work (dispersion and repulsion energy). A conventional set of Pauling radii and a tetrahedral cavity with 64 initial tesserae were used in the CPCM calculations. The above treatment, i.e., continuum model calculations based on optimized clusters, which partially account for local solvation by explicitly including several solvent molecules in an inner solvation shell, is called the cluster-continuum model.[22] All quantum chemistry calculations were performed with Gaussian 03, version 1.0.[23]

2.2. MD Procedure. Classical molecular dynamics simulations were performed with the DL_POLY program, version 2.14.[24] An initial configuration consisting of a 12-mer chain of polyphosphazene (**1**) was optimized by molecular mechanics,

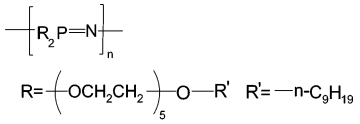

1

using the UFF force field in a super cell of (64.8 × 32.0 × 10.2) Å^3. Twenty-four water and 12 $Li^+CF_3SO_3^-$ molecules were randomly distributed in the box, with initially large separations between the Li^+ cations and the $CF_3SO_3^-$ anions. The canonical NVT ensemble (T = 300 K) was sampled by using the Evans thermostat.[25] The equations of motion were integrated by the Verlet leapfrog algorithm, with a time step size of 1 fs. The overall system was initially equilibrated for 500 ps, followed by another 600 ps for data collection.

The DREIDING/A many-body force field,[26] consisting of two-body bond stretch, three-body bond-angle bend, four-body dihedral angle torsion and inversion, and nonbonded interactions, was employed for the 12-mer PP and for the triflate anion; some changes were introduced to model PP mer−triflate anion charges. The SPC model potential was used for water.[27] The charge of the Li^+ cation was set to 1; its van der Waals parameters were taken from Peng et al.[28] Partial atomic charges for $CF_3SO_3^-$ were obtained by fitting the molecular electrostatic potential (ESP) of the optimized B3PW91/6-31G* geometry. To estimate reasonable charges for the 12-mer PP structure, calculations were performed on the model molecule (**2**) and partial atomic charges were calculated by fitting its ESP.

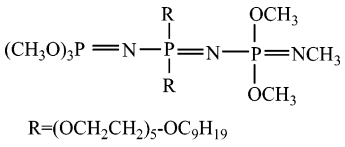

(**2**)

3. Results and Discussions

3.1. Hydration of Li^+ and $CF_3SO_3^-$. Li^+-water clusters ($Li^+(H_2O)_{1-6}$) were fully optimized for comparison with interactions of Li^+ with other species in the PP polymer electrolyte. The preferred geometries of the clusters are in good agreement with optimal geometries determined in previous studies.[14] Water molecules in the first solvation shell align their dipoles radially toward the central Li^+, and tend to array themselves in high symmetry to minimize mutual repulsions. This packing allows up to four water molecules in the first shell. Extra water molecules locate in a second shell, and interact with the water molecules in the first shell via hydrogen bonds, as shown in Figure 1, **1a** and **1b**, for $Li^+(H_2O)_5$ and $Li^+(H_2O)_6$. Structure **1c** shows a local minimum in which Li^+ complexes with 6 waters in the first shell; it is less favorable than structure **1b** by approximately 8.0 kcal/mol. The variations of ΔH at B3PW91/6-311++G(d,p)//B3PW91/6-31G* from $Li^+(H_2O)_4$ to $Li^+(H_2O)_5$ and from $Li^+(H_2O)_5$ to $Li^+(H_2O)_6$ (**1b**) are 11.8 and 9.7 kcal/mol, respectively, which are approximately double the values of the water dimerization energy (−4.7 to −5.1 kcal/mol,[36,37] exptl −5.4 ± 0.7 kcal/mol[38]), suggesting that the two excess water molecules predominantly interact with the first shell water molecules via two hydrogen bonds.

TABLE 1: Distances between Li^+ and a Water Oxygen (R/Å), Enthalpies (ΔH, kcal/mol) and Gibbs Free Energies (ΔG, kcal/mol) of Formation of $Li^+(H_2O)_n$ at Various Theoretical Levels

	HF/6-31G*			B3PW91/6-311++G(d,p)//HF/6-31G*		B3PW91/6-31G*				B3PW91/6-311++G(d,p)//B3PW91/6-31G*		
n	R	ΔH^a	ΔG^a	ΔH^b	ΔG^b	R	ΔH^a	ΔG^a	$q(Li^+)$	ΔH^c	ΔG^c	exptl ΔH^d
1	1.858	−36.5	−29.6	−34.2	−27.4	1.853	−36.2	−29.9	0.98	−34.2	−27.8	−34.0
2	1.883	−67.0	−53.1	−63.6	−48.8	1.878	−66.4	−52.1	0.99	−62.9	−48.6	−59.8
3	1.918	−87.1	−65.2	−84.1	−62.2	1.914	−88.5	−67.0	0.98	−84.0	−62.4	−80.5
4	1.970	−105.9	−76.4	−98.5	−69.0	1.967	−103.0	−73.2	0.88	−97.9	−68.1	−96.9
5[f]	1.965/3.798	−116.5	−77.6	−110.3	−70.2	1.96/3.641	−116.3	−77.8	0.88	−109.7	−71.2	−110.8
6	1.968/3.833	−127.3	−78.5	−120.2	−71.2	1.965/3.663	−128.4	−77.1	0.86	−119.8	−68.4	−122.9
6[e]	2.153	−115.0	−66.5									

[a] $Li^+ + nH_2O \rightarrow Li^+(H_2O)_n$: $\Delta H = H[Li^+(H_2O)_n] - H(Li^+) - nH(H_2O) + BSSE$; likewise for ΔG. [b] $\Delta H = \Delta E$[B3PW91/6-311++G(d,p)//HF/6-31G*] + the enthalpy correction (HF/6-31G*); likewise for ΔG. [c] $\Delta H = \Delta E$[B3PW91/6-311++G(d,p)//B3PW91/6-31G*] + the enthalpy correction (B3PW91/6-31G*). [d] Reference 29. [e] Conformation **1c**. [f] R data indicated after a slash refer to the distances between Li^+ and the second shell water oxygen.

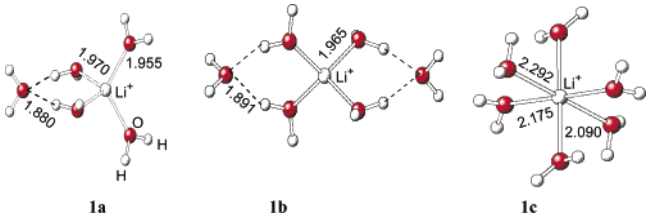

Figure 1. B3PW91/6-31G* optimized clusters: $Li^+(H_2O)_5$ (**1a**) and $Li^+(H_2O)_6$ (**1b**, **1c**).

Table 1 lists the distances between Li^+ and water oxygens (R, Å), and cumulative enthalpies (ΔH) and Gibbs free energies (ΔG), with BSSE corrections for the formation of $Li^+(H_2O)_n$ clusters. HF/6-31G* and B3LYP/6-31G* predict identical values of R for the first solvation shell; however, the R values optimized by HF for the second shells of $Li^+(H_2O)_5$ and $Li^+(H_2O)_6$ are approximately 0.15 Å longer than those predicted by B3LYP. Both ΔH and ΔG, with B3PW91/6-311++G(d,p) using the geometries respectively optimized by HF/6-31G* and B3PW91/6-31G*, agree within 0.5 kcal/mol up to $Li^+(H_2O)_3$. This means that HF/6-31G* describes strong interactions, such as those between Li^+ and a water oxygen, adequately, but is insufficiently accurate for the water−hydrogen bonding systems. The two methods result in 1−3 kcal/mol ΔG differences for $Li^+(H_2O)_{4-6}$. It is interesting to note that the calculated ΔH values from B3PW91/6-311++G(d,p)//HF/6-31G* and B3PW91/6-311++G(d,p)//B3PW91/ 6-31G* are in good agreement with the experimental data;[29] the average absolute error is less than 2.0 kcal/mol.

As illustrated in Figure 2, structures **2a** and **2b**, the anion $CF_3SO_3^-$ can be hydrated through two types of weak hydrogen bonds, $O^{\delta-}\cdots H-OH$ and $F^{\delta-}\cdots H-OH$. The former is considerably stronger than the latter, which is qualitatively in line with the charges carried by the oxygen and the fluorine atoms of the anion respectively, −0.58e vs −0.14e, calculated with B3PW91/6-31G*. The difference in binding strengths is also reflected by the 0.15 Å longer distances from F than from O to the water hydrogen. It has been reported that the hybrid exchange functional B3 is unable to describe weak interacting systems;[30] however, the exchange functional PBE [31] with the large basis set 6-311++G(d,p) (PBEPBE/6-311++G(d,p) in Table 2) does not improve much over B3PW91/6-31G* for $CF_3SO_3^-(H_2O)_{1-2}$. Compared with the structure of hydrated Li^+, the $CF_3SO_3^-(H_2O)_n$ clusters are less tight, i.e., the distance from the water hydrogen to the anion oxygen ($O^{\delta-}\cdots H_2O$) is about 0.2 Å longer than that from the water oxygen to Li^+ ($Li^+\cdots OH_2$) (2.1 vs. 1.9 Å). In the cases of three or more water molecules, structures **2d**−**f**, some distances from the water hydrogen to the anion oxygen become shortened, to approximately 1.85 Å, due to the cooperative effect of the hydrogen bonds. The $O^{\delta-}\cdots H-OH$ is enhanced by the presence of the second hydrogen bond between water molecules.

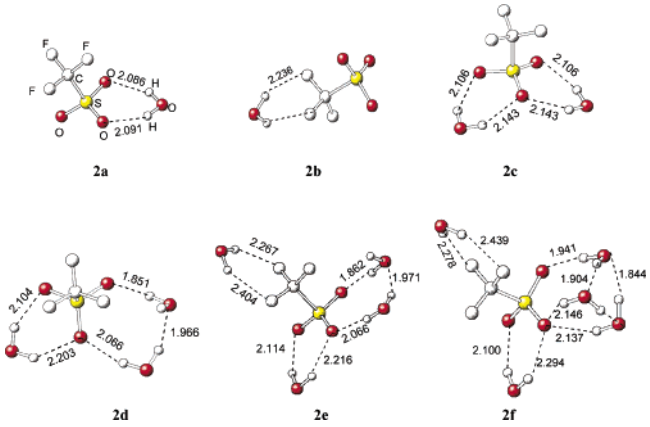

Figure 2. B3PW91/6-31G* optimized anion−water clusters $CF_3SO_3^-(H_2O)_{1-5}$. The dotted lines indicate hydrogen bonds between water and the anion or among water molecules; all the lengths are in Å.

TABLE 2: Thermodynamics of Triflate Anion Clusters $CF_3SO_3^-(H_2O)_n$[a]

		B3PW91/6-31G(d)		PBEPBE/6-311++G(d,p)	
n	geometries	$-\Delta H^b$	$-\Delta G^b$	$-\Delta H$	$-\Delta G$
1	**2a**	9.9	4.5	11.0	3.9
1	**2b**	2.7	−0.8		
2	**2c**	18.1	7.2	20.6	6.3
3	**2d**	25.4	9.5		
4	**2e**	26.4	7.4		
5	**2f**	36.3	12.0		

[a] Enthalpies (ΔH) and free energies (ΔG) in kcal/mol. [b] $CF_3SO_3^- + nH_2O \rightarrow CF_3SO_3^-(H_2O)_n$: $\Delta H = H[CF_3SO_3^-(H_2O)_n] - H(CF_3SO_3^-) - nH(H_2O) + BSSE$; BSSE was not included in ΔG.

In general, $CF_3SO_3^-$ hydration energy, measured in terms of enthalpy of formation of water-containing clusters, is considerably weaker than that of Li^+ cation, i.e., −10 vs. −36 kcal/mol and −25 vs. −88 kcal/mol for one and three coordinated water molecules. The former represents approximately one-third of the Li^+ hydration enthalpy. Thus, it is expected that anion hydration will play a nonnegligible role in the dissociation of lithium triflate.

3.2. Hydration of $LiCF_3SO_3$. To investigate the $CF_3SO_3^-$−Li^+ ion pairing, saltwater clusters $[LiCF_3SO_3(H_2O)_{0-7}]$ were fully optimized. Although all three types of coordination (monodentate, bidentate, and tridentate) are indeed found for $LiCF_3SO_3$ at the HF/3-21G level, the bidentate (Figure 3,

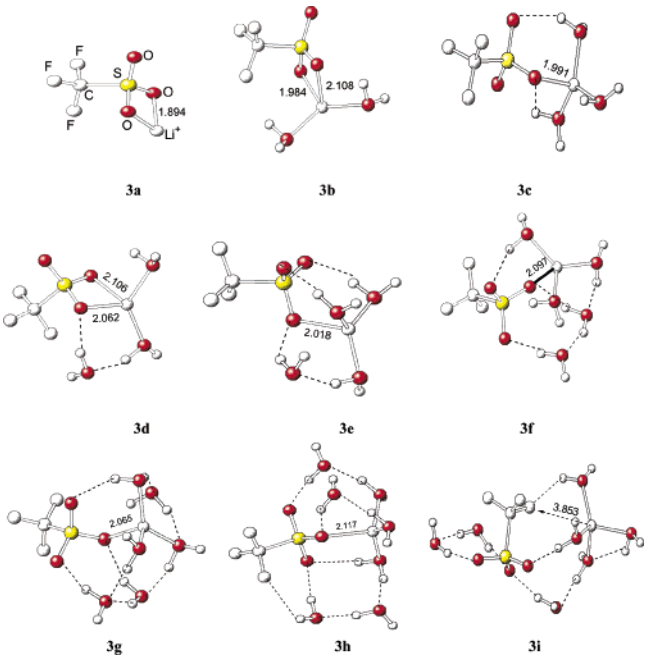

Figure 3. Optimized structures at the B3PW91/6-31 level for the ion pair ($LiCF_3SO_3$) and its binary aggregates with water molecules, $LiCF_3SO_3-(H_2O)_{0-7}$. The numbers refer to the distances (in Å) from Li^+ to the coordinated anion oxygens, and the dotted lines indicate hydrogen bonds between water and the anion or among water molecules.

structure **3a**) is the sole stable structure at higher levels of approximation, such as HF/6-31G* and B3PW91/6-31G*. This is in agreement with the corresponding results of Johansson et al.[13] When $CF_3SO_3^-$—Li^+ is solvated by three or more water molecules in isolated clusters, monodentate structures with respect to the coordination of Li^+ and the triflate anion become favorable, because the interaction of Li^+ and water probably compensates for the difference between monodentate and bidentate coordination. Structure **3c**, for example, has approximately 6.0 kcal/mol lower energy than **3d**. In **3d**, the distances of Li^+ to the coordinated anion oxygen atoms are considerably stretched compared with the gas-phase bidentate structure (2.106, 2.062 vs 1.893 Å). Patterns where Li^+ prefers to be single coordinated to the triflate anion, forming a solvated CIP, are also found for high degrees of hydration, as shown in structures **3e**—**h**. When more than three water molecules solvate $LiCF_3SO_3$, the excess water molecules interact with the water molecules in the first solvation shell of Li^+, as well as with the anion oxygen atoms, via hydrogen bonds. For seven water molecules, one water molecule clearly interacts with the anion F atom, as shown in structure **3h**. Table 3 shows that the distances from Li^+ to its nearest anion oxygen (R_{Li-O-X}) increase with the number of water molecules, and reach values of approximately 2.10 Å in $LiCF_3SO_3(H_2O)_7$ clusters. This means that the CIP is weakened by local hydration. This can be further confirmed by examining the ΔG_{diss} in Table 3. However, complete dissociation (conversion into a solvent-separated IP) requires an even higher degree of solvation. The precise solvation that can dissociate $LiCF_3SO_3$ is under investigation with quantum molecular dynamics, by including still more solvent molecules.

In addition, a solvent-shared ion pair (SSIP) was also located for $LiCF_3SO_3(H_2O)_7$, as shown in structure **3i**, where the Li^+ cation is separated from the anion by 3.853 Å, the distance from Li^+ to the nearest anion oxygen atom. In structure **3i**, three water molecules simultaneously solvate Li^+ and the anion $CF_3SO_3^-$. The SSIP is 20.9 kcal/mol higher in energy than the solvated CIP (structure **3h**).

The thermodynamics of local hydration of $LiCF_3SO_3$ and the dissociation of the clusters $LiCF_3SO_3(H_2O)_{0-7}$ in a vacuum and bulk solvent are systematically investigated and summarized in Table 3 for the following two reactions,

$$LiCF_3SO_3 + nH_2O \rightarrow LiCF_3SO_3(H_2O)_n \quad (1)$$

$$LiCF_3SO_3(H_2O)_n \rightarrow Li(H_2O)_m + CF_3SO_3(H_2O)_{n-m} \quad (m = n \text{ as } n \le 4;\ m = 4 \text{ as } n > 4) \quad (2)$$

The corresponding Gibbs free energy variations are respectively defined by

$$\Delta G_{hyd} = G[LiCF_3SO_3(H_2O)_n] - G(LiCF_3SO_3) - nG(H_2O) \quad (3)$$

$$\Delta G_{diss} = G[Li(H_2O)_m] + G[CF_3SO_3(H_2O)_{n-m}] - G[LiCF_3SO_3(H_2O)_n] \quad (4)$$

To incorporate the bulk solvent effect, the corresponding solvation energies (G_{sol}) need to be added into eq 4, and for the dissociation of the clusters $LiCF_3SO_3(H_2O)_{0-7}$ yields

$$\Delta G = \Delta G_{diss} + G_{sol}[Li(H_2O)_m] + G_{sol}[CF_3SO_3(H_2O)_{n-m}] - G_{sol}[LiCF_3SO_3(H_2O)_n] = \Delta G_{diss} + \Delta G_{sol} \quad (5)$$

Table 3 shows that the local hydration of $LiCF_3SO_3$ is spontaneous for values of n up to seven water molecules. Significant decreases of ΔG_{hyd} for $LiCF_3SO_3(H_2O)_{2-3}$ are caused by the strong interaction between Li^+ and the water oxygen, whereas hydrogen bonding between the excess water molecules and the water molecules in the first solvation shell, as well as with the anion group, are responsible for the consequent gentle decrease of ΔG_{hyd} for $LiCF_3SO_3(H_2O)_{4-7}$. Consistent with the trend reflected by the distances of Li^+ to the nearest anion oxygen, R_{Li-O-X}, ΔG_{diss} decreases approximately by 53 kcal/mol from $LiCF_3SO_3$ to $LiCF_3SO_3(H_2O)_7$, indicating that the interaction between the cation and anion domains is dramatically weakened by hydrations of Li^+ and the anion.

Bulk solvent corrections were introduced by the CPCM method for high and low polarity media, $\epsilon = 78.0$ and 10.0, respectively, the former mimicking water and the latter a PP polymer environment. Considerably high solvation free energies (G_{sol}) are predicted for both the cation and the anion clusters, $Li^+(H_2O)_m$ and $CF_3SO_3^-(H_2O)_{n-m}$. For instance, in the case of $\epsilon = 78.0$, G_{sol} of $Li^+(H_2O)_4$ and $CF_3SO_3^-(H_2O)_3$ are respectively −62.4 and −58.1 kcal/mol, for which the local hydration free energies shown in Tables 1 and 2 were −73.2 and −9.5 kcal/mol. Thus, the water-containing clusters are still far from full hydration, especially the anion—water complex, $CF_3SO_3^-(H_2O)_3$. G_{sol} of $CF_3SO_3^-$ is roughly half that of Li^+ (−67.6 vs. −116.4 kcal/mol), indicating that the anion is considerably stabilized by hydration and that (as discussed in a previous section) the anion hydration will play a very important role in the dissociation of lithium triflate. The spontaneous dissociation of $LiCF_3SO_3$ in bulk water is demonstrated by the negative total dissociation free energies (ΔG, the last column in Table 3). It is also noted that the ΔG values calculated with the cluster—CPCM model are from a few to 10 kcal/mol lower than ΔG values obtained with CPCM for naked $LiCF_3SO_3$.

TABLE 3: Distances between Li^+ and the Nearest Anion Oxygen (R_{Li-O-X}/Å) in the Hydrated XLi, $XLi(H_2O)_{0-7}$ (X = $CF'_3SO_3^-$), Cumulative Gibbs Free Energies of Hydration (ΔG_{hyd}, kcal/mol) in Vacuum Phase, Gibbs Free Energies of Dissociation of the Hydrated Cluster into Hydrated Li^+ and Anion X^- in Vacuum (ΔG_{diss}), Gibbs Free Energies of Solvation for the Involved Species Predicted with the CPCM Model(G_{sol}, kcal/mol), and Total Gibbs Free Energies of Dissociation Predicted by the Cluster-CPCM Method ($\Delta G = \Delta G_{sol} + \Delta G_{diss}$) at theB3PW91/6-31G* Level

$LiCF_3SO_3(H_2O)_n$						G_{sol}[d]				
n	*m*	geometry	R_{Li-O-X}[a]	ΔG_{hyd}[b]	ΔG_{diss}[c]	$XLi(H_2O)_n$	$Li^+(H_2O)_m$	$X(H_2O)_{n-m}$	ΔG_{sol}[e]	ΔG[f]
0	0	**3a**	1.893(2)		142.8	−36.9	−116.4	−67.6	−147.1	−4.3
1	1		1.930(2)	−15.9 (−15.2)	125.8	−31.4	−95.0	−67.6	−131.2	−5.4
2	2	**3b**	2.046(2)	−23.1 (−24.0)	107.1	−26.0	−78.0	−67.6	−119.6	−12.5
3	3	**3c**	1.991	−32.7 (−30.0)	98.2	−23.3	−67.2	−67.6	−111.5	−13.3
4	4	**3e**	2.018	−36.0 (−31.8)	91.3	−22.0	−62.4	−67.6	−108.0	−16.7
5	4	**3f**	2.097	−41.1 (−33.7)	91.8	−21.0	−62.4	−60.6	−102.0	−10.2
6	4	**3g**	2.088	−43.3	91.4	−20.6	−62.4	−57.9	−99.7	−8.3
7	4	**3h**	2.117	−43.8	89.6	−24.4	−62.4	−58.1	−96.1	−6.5
7	4	**3i**	3.853		71.4	−36.7	−62.4	−58.1	−83.8	−12.2
0[g]	0	**3a**	1.893(2)		142.8	−32.7	−105.8	−58.6	−131.7	11.1
3[g]	3	**3c**	1.991	−32.7	98.2	−20.0	−60.7	−58.6	−99.3	−1.1
4[g]	4	**3e**	2.018	−36.0	91.3	−18.8	−56.1	−58.6	−95.9	−4.6
4[h]	4	**3e**	2.018	−36.0	91.3	−13.5	−45.1	−48.9	−80.6	10.7

[a] The number in parentheses refers to the coordination number of Li^+ with triflate anion, otherwise it is one. [b] $LiCF_3SO_3 + nH_2O \rightarrow LiCF_3SO_3(H_2O)_n$; the data in parentheses refer to those with HF/6-31G*. [c] $LiCF_3SO_3(H_2O)_n \rightarrow CF_3SO_3^- + Li^+(H_2O)_n$ for $n \leq 4$; $LiCF_3SO_3(H_2O)_n \rightarrow CF_3SO_3^-(H_2O)_{n-4} + Li^+(H_2O)_4$ for $n > 4$. [d] $m = n$ as $n \leq 4$; $m = 4$ as $n > 4$; predicted by the CPCM model with Pauling radii and dielectric constant = 78.0 unless specified. [e] $\Delta G_{sol} = G_{sol}[X(H_2O)_{n-m}] + G_{sol}[Li(H_2O)_m] - G_{sol}[XLi(H_2O)_n]$. [f] $\Delta G = \Delta G_{diss} + \Delta G_{sol}$. [g] For CPCM, dielectric constant = 10.0. [h] For CPCM, dielectric constant = 4.0.

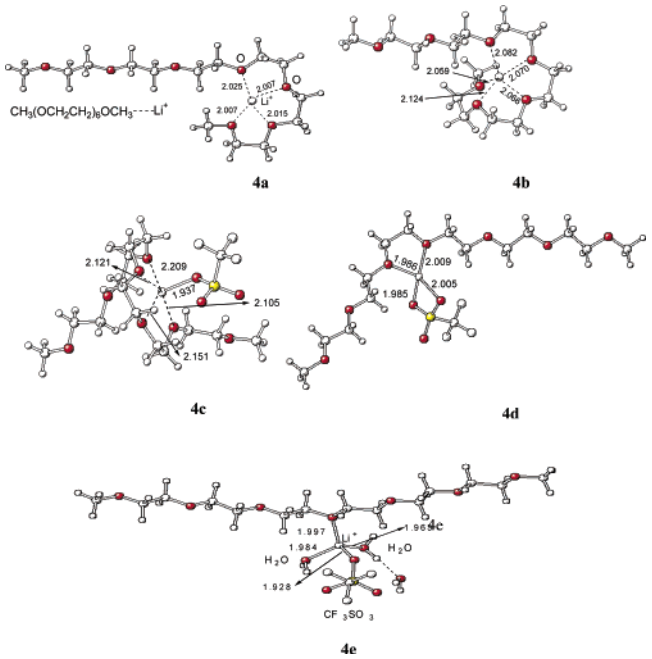

Figure 4. Optimized structures at the HF/6-31G* level: four- and five-coordinated complexes of Li^+ with $(EO)_6$ (**4a** and **4b**), binary aggregates of $LiCF_3SO_3-(EO)_6$ (**4c** and **4d**), and ternary aggregate $LiCF_3SO_3-(EO)_6-(H_2O)_3$ (**4e**).

The variation of G_{sol} and consequent ΔG in the low polar medium ($\epsilon = 10$) is qualitatively analogous to that found in the more highly polar medium. The positive ΔG for the naked CIP (11.1 kcal/mol), which is reduced respectively to −1.1 and −4.6 kcal/mol for $LiCF_3SO_3(H_2O)_{3-4}$, further implies that the cluster−CPCM treatment is essential to properly describe the solvent effect. A lower polarity medium ($\epsilon = 4$) decreases the dissociation ability of $LiCF_3SO_3(H_2O)_{3-4}$, as evidenced by its positive ΔG, 10.7 kcal/mol. In brief, the cluster−CPCM calculations show that the CIP is likely to be dissociated into solvated ions even in low polarity media like PEO and PP polymers.

3.3. Interactions of Li^+ and $CF_3SO_3^-$−Li^+ with Poly(ethylene oxide) (PEO) Fragments in the Presence of Water.

TABLE 4: Averaged Distances (Å) between Li^+ and Ether Oxygen Atoms (R_{Li-O}/Å) in the $(EO)_6-Li^+$ Complexes, Binding Energies (ΔE, ΔE_0/kcal/mol), Enthalpies (ΔH), and Gibbs Free Energies (ΔG) of Formation of the Complexes Calculated with HF/6-31G*

coord no.	R_{Li-O}	ΔE[a]	ΔE_0[b]	ΔH[c]	ΔG[c]	$\Delta\Delta G$
1	1.84	−39.4	−36.4	−36.8	−30.1	
2	1.88	−65.9	−60.6	−61.6	−53.1	−23.0
3	1.93	−86.3	−79.8	−80.2	−70.0	−16.9
4[d]	2.01	−101.3	−92.2	−94.0	−82.0	−12.0
5[e]	2.08	−110.3	−100.2	−102.3	−88.3	−6.3
6	2.25	−111.5	−101.3	−103.4	−89.3	−1.1

[a] ΔE is the energy of the complex relative to Li^+ cation and the all-trans conformer for $CH_3O(CH_2CH_2O)_6-CH_3$; the values are almost the same as reported in the literature with different models for some coordinations: $CH_3O(CH_2CH_2O)_2CH_3$ for 1−3 coordination, and $CH_3O(CH_2CH_2O)_{3-5}CH_3$ for 4, 5, and 6 coordination, respectively.[b] ΔE_0 = ΔE + zero point energy correction + BSSE; BSSE values are respectively 2.0, 3.1, 4.6, 5.6, 6.1, 6.2 kcal/mol for $n = 1-5$ at HF/6-31G*. [c] BSSE are included. [d] Conformation **4a** in Figure 4. [e] Conformation **4b** in Figure 4.

To determine the strength of the interactions of Li^+ with the side chain of the polyphosphazene polymer and to predict the microstructure surrounding the ion when located near this side chain, $CH_3O(CH_2CH_2O)_6CH_3$ [$(EO)_6$] was used as a model of the side chain of a MEEP-like PP. Li^+ is able to coordinate with multiple adjacent ether oxygen atoms by twisting CH_2CH_2O groups from all-trans conformations.[9,10,15,35] Four- and five-coordinated complexes are illustrated in Figure 4, structures **4a** and **4b**. For comparison with previous reports, the binding energies (ΔE) without zero point energy correction and BSSE are also given in Table 4 along with other characteristics. The ΔE values are almost the same as those reported by the Curtiss group,[15] although inconsistent models were used there for some coordinations: $CH_3O(CH_2CH_2O)_2CH_3$ for coordination with one to three oxygen atoms, and $CH_3O(CH_2CH_2O)_{3-5}CH_3$ for four- to six-coordination, respectively. It should be noted that although the binding energies and enthalpies of formation still decrease from five- to six-coordinate species, the small decrease of ΔG (∼1 kcal/mol) implies that Li^+ is most likely to interact only with five sites in the first shell. This supports a few recent

TABLE 5: Distances from Li^+ to the Nearest Anion Oxygen (R_{Li-O-X}/Å), to the Ether Oxygen of $(EO)_6$ ($R_{Li-O-EO}$), and to the Water Oxygen (R_{Li-O-W}) in the Aggregates $LiX(H_2O)_{0-3}(EO)_6$, and Their Binding Energies (ΔE/kcal/mol), Enthalpies (ΔH), and Gibbs Free Energies (ΔG) of Formation at 298.2 K with HF/6-31G*

conformations	structure	R_{Li-O-X}[d]	$R_{Li-O-EO}$[c]	R_{Li-O-W}	ΔE[a]	ΔE_0[b]	ΔH	ΔG
$(EO)_6-LiX$		1.94	1.91		−22.2	−21.3	−20.6	−11.9
$(EO)_6-LiX$	**4c**	2.147(4)	1.94		−39.1	−36.6	−37.1	−21.7
$(EO)_6-LiX$	**4d**	2.00(2)	2.00(2)		−34.1	−32.5	−32.2	−20.7
$(EO)_6-LiX-H_2O$		2.02(2)	1.97	1.99	−39.8	−36.8	−36.5	−19.5
$(EO)_6-LiX-(H_2O)_2$		1.94	1.98	2.00	−58.5	−52.3	−53.0	−24.4
$(EO)_6-LiX-(H_2O)_3$	**4e**	1.95	2.00	1.99	−72.8	−64.0	−65.3	−27.4

[a] $\Delta E = E$ (aggregate) $- E$ ($LiCF_3SO_3$) $- mE(H_2O) - E$[*all-trans*-$CH_3O(CH_2CH_2O)_6-CH_3$]. [b] $\Delta E_0 = \Delta E$ + ZPE. [c] The number in parentheses refers to the coordination number of Li^+ with the triflate anion, otherwise it is one. [d] The number in parentheses refers to the coordination number of Li^+ with $(EO)_6$, otherwise it is one.

experimental findings. Using X-ray diffraction, Bruce et al. found that Li^+ is accommodated within the PEO helix by coordination with 5 ether oxygens in the crystalline PEO_6LiXF_6 (X = P, Sb).[32,33] Mao et al. determined the local structure of Li^+ in amorphous $PEO_{7.5}LiClO_4$ by neutron diffraction, suggesting that Li^+ is predominantly coordinated by 4−5 ether oxygens.[39] The distances between Li^+ and the oxygen atom of the five-coordinated complex (**4b**) are comparable to those in PEO_6:$LiPF_6$ (2.06−2.12 vs 2.17−2.18 Å[33]) and in $PEO_{7.5}LiClO_4$ (2.07 ± 0.04 Å[39]). Comparing Tables 1 and 4, it can be found that both the distances of Li^+ to oxygen and ΔG for the one- and two-coordination cases of the two systems, Li^+-H_2O and $Li^+-(EO)_6$, are almost the same, indicating that the interactions of Li^+ are comparable with those of the ether and water oxygen atoms. Because of their smaller entropy loss, the ΔG values of the three and four-coordination complexes for the $Li^+-(EO)_6$ system are approximately 5−6 kcal/mol more negative than those of the Li^+-H_2O system.

Binary aggregates of the CIP and $(EO)_6$, $(EO)_6-Li^+CF_3SO_3^-$ (structures **4c** and **4d**), were located. Structural parameters and thermodynamics are summarized in Table 5. The ΔG values of the one-, two-, and four-coordination compounds of $(EO)_6-LiCF_3SO_3$ are respectively 3.8, 3.7, and 10.1 kcal/mol less negative than those of $H_2O-LiCF_3SO_3$ (−11.9, −20.7 ,and −21.7 vs. −15.7, −24.0, and −31.8 kcal/mol at the HF/6-31G* level). This suggests that $(EO)_6$, our model for the side group of a MEEP-like PP, has less ability to solvate the CIP. Such binary aggregates, $(PEO)MCF_3SO_3$ (M = Na, Li), were observed for the systems $(PEO)_nMCF_3SO_3$ ($n = 1-80$) by Frech et al. using Raman and FTIR spectroscopy.[8] They pointed out that the binary aggregate clearly becomes the dominant species over solvated ions and ion pairs in the concentration range from 20:1 to 1:1 (PEO: salt). The spontaneous formations of **4c** and **4d** evidenced by the considerably negative ΔG values (−21.7 and −20.7 kcal/mol) support the presence of binary aggregates, $(PEO)-MCF_3SO_3$, in the polymer electrolyte $PEO_nMCF_3SO_3$. The present thermodynamic data for the formation of the binary aggregate $(EO)_6-LiCF_3SO_3$ basically support Frech's findings. As water was introduced into the $CF_3SO_3Li-PEO$ system, stable ternary aggregates consisting of water, CIP, and $(EO)_6$, $CF_3SO_3Li-(H_2O)_{1-3}-(EO)_6$, were also located as shown in structure **4e** for $CF_3SO_3^-Li^+-(H_2O)_3-(EO)_6$. As reflected by the ΔG of formation for the ternary aggregates, the binary aggregates $CF_3SO_3^-Li^+-(EO)_6$ can be further hydrated spontaneously by up to three water molecules. Thus, ternary aggregates are most likely to be present near the side chain of PP at medium salt concentrations.

3.4. Interactions of Li^+ and $CF_3SO_3^-Li^+$ with the Polyphosphazene Backbone in the Presence of Water. Initially, $CH_3[N{=}P(CH_3)_2]_3CH_3$ (PP3) (Figure 5, structure **5a**) was used as a model for the backbone of polyphosphazene. It prefers a periodic gauche−trans conformation around the N−P bond. Multiple interactions of Li^+ with N atoms are possible, as shown in structures **5b** and **5c** for one- and two-coordination complexes. Binding energies of Li^+ with N atoms are higher than those of Li^+ with the ether oxygen for a given coordination number, for example, the ΔE values are 51.7 and 39.4 kcal/mol, respectively, for the single coordination, which is consistent with the charge difference carried by nitrogen and the ether oxygen (−1.17e vs. −0.66e). To confirm this energy difference, complexes were also optimized for Li^+ and another model of a MEEP-like PP, $CH_3[N{=}P(OCH_3)_2]_6OCH_3$ (PP6) (Figure 6, structure **6a**), in which the phosphorus atoms link with two methoxy groups rather than with two methyl groups (in PP3).

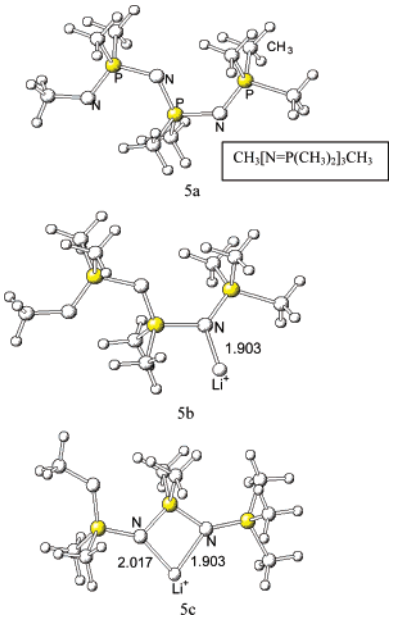

Figure 5. $CH_3[N{=}P(CH_3)_2]_3CH_3$ (PP3) (**5a**) and its complexes with Li^+ (**5b** and **5c**) optimized with HF/6-31G*.

The averaged bond angles of NPN, OPO, OPN, and PNP are 117°, 103°, 110°, and 120°, respectively; the first three significantly deviate from the suggested bond angle for the sp^3 hybridized phosphorus in the DREIDING force field.[26] Because of the closeness of the nitrogen and its neighboring methoxy oxygen atoms (~2.5 Å), Li^+ is able to triply coordinate with one nitrogen and two methoxy oxygen atoms as shown in structure **6b**, forming the so-called pocket structure proposed by Luther.[11] Another two three-coordination complexes of Li^+ are also shown in Figure 6, structures **6c** and **6d**, interacting respectively with two next-neighboring nitrogen atoms and one methoxy oxygen, and with three nitrogen atoms (two adjacent and one next neighboring). The stability of the three-coordination complexes increases in the following order: **6b** < **6d** <

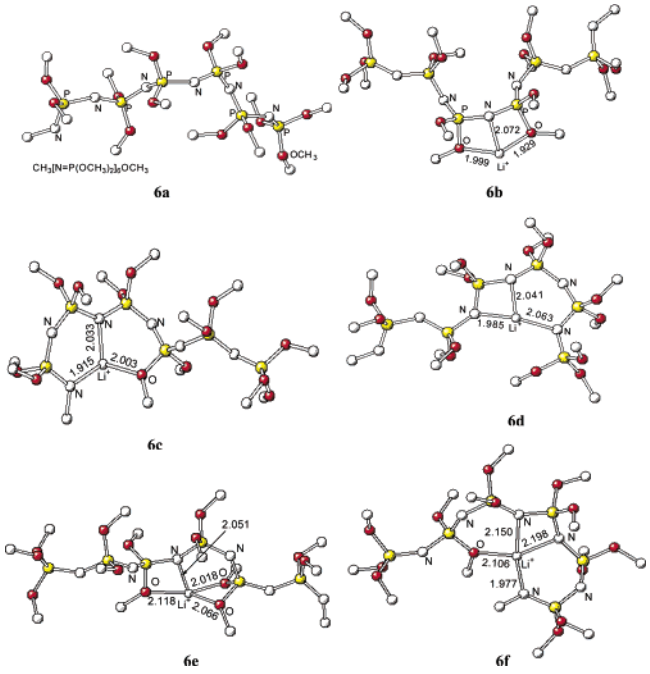

Figure 6. Optimized structures with HF/6-31G* for $CH_3[N{=}P(OCH_3)_2]_6$-OCH_3 (PP6) (**6a**) and a variety of its complexes with Li^+ (**6b**−**f**). For clarity, hydrogen atoms are not shown.

6c ($\Delta E = -83$, -105, and -132 kcal/mol). The stronger interaction found between Li^+ and the backbone nitrogen compared with that of Li^+ with the methoxy oxygen is most likely responsible for the stability difference between **6b** and **6d**. However, the extra stability of **6c** may be due to the two six-membered rings, since its strain is much lower than that of the four-membered ring, one and two of which are present in **6d** and **6b**, respectively. As shown in structures **6e** and **6f**, four-coordination complexes were also located. Again the pocket structure (**6e**) (Li coordinating with one nitrogen and three methoxy oxygen atoms; $\Delta E = -95$ kcal/mol) is less stable, and the favorable structure is **6f** where three Li−N and one Li−O bond lengths are 1.977, 2.150, 2.198, and 2.106 Å, respectively. In brief, the preferred coordinations of Li^+ with PP6 involve multiple (2−3) next neighboring nitrogen atoms and one methoxy oxygen, such as **6c** and **6f**, both featuring a high coordination number and low strain conformation (six-membered ring).

For a given Li^+ coordination number, Figure 7 illustrates the Gibbs free energies of formation of Li^+ complexes for H_2O, $(EO)_6$, and PP6, showing that the backbone fragment of PP6 interacts most strongly with Li^+ via both nitrogen atoms and an adjacent ether oxygen atom, and that the interaction between Li^+ and $(EO)_6$ is slightly stronger than that between Li^+ and H_2O for three and larger coordination complexes.

Similarly to the case of $(EO)_6$, binary aggregates of PP6 and the CIP (PP6−$LiCF_3SO_3$) were also located as shown in Figure 8, structures **8a**−**c**. Thermodynamic data reported in Table 6 show that PP6 has a stronger tendency to form binary aggregates with triflate lithium than both water and $(EO)_6$ do. For instance, the ΔG (relative to the fragments PP6/water/$(EO)_6$ and the CIP) for the aggregates **3b**, **4d**, and **8b**, in which Li^+ is doubly coordinated with the fragments via the water oxygen, the ether oxygen, and the nitrogen atoms, are -24.0, -20.7, and -27.5 kcal/mol, respectively. The strongest interaction causes the largest separation of the CIP, reflected by the elongated R_{Li-O-X} distance (2.05 vs. 2.03 and 2.00 Å in **8b**, **3b**, and **4d** at the HF/6-31G* level), although such interaction could not completely dissociate the CIP either. The combination of one water molecule with the binary aggregate **8b** gives rise to a ternary aggregate $CF_3SO_3Li-H_2O-PP6$, as shown in structure **8d**, where Li^+ is singly coordinated with the anion. Starting with **8c**, the corresponding ternary aggregate is also located (**8e**, not shown), in which Li^+ coordinates with two backbone N atoms, a water oxygen, and one oxygen of the anion. The formations of **8d** and **8e** are spontaneous, as evidenced by their more negative ΔG values than those of **8b** and **8c** (-36.5 vs. -27.5 kcal/mol; -48.1 vs. -43.2 kcal/mol). Thus, the most favorable conformation of Li^+ near the backbone of PP is that where $LiCF_3SO_3$ interacts with one and two nitrogen atoms through a $Li^+\cdots N$ and simultaneously Li^+ interacts with at least one water molecule in the first solvation shell.

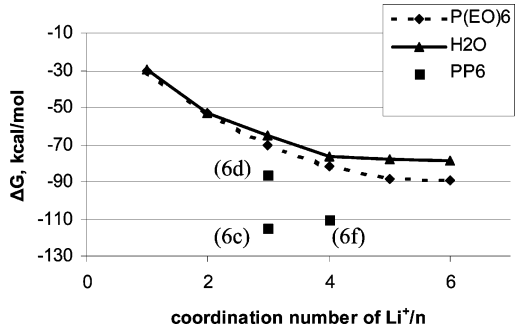

Figure 7. Gibbs free energies (ΔG) of formation of Li^+ complexes with $(EO)_6$, H_2O, and PP6.

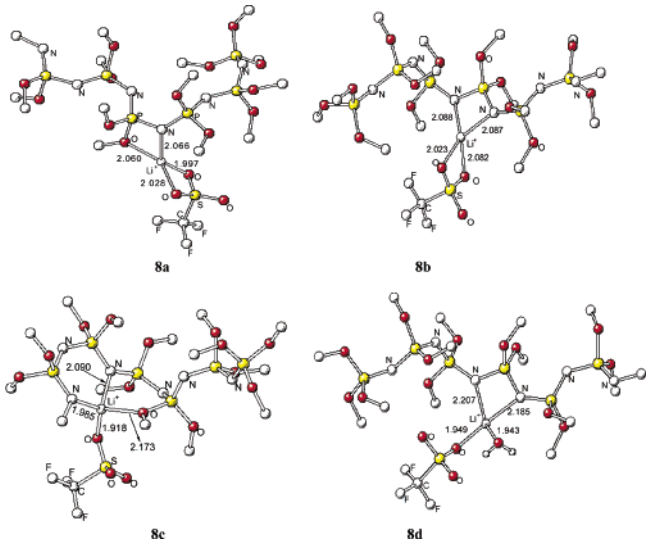

Figure 8. Binary aggregates of $LiCF_3SO_3-CH_3[N{=}P(OCH_3)_2]_6OCH_3$ (PP6) (**8a**−**c**) and ternary aggregate $LiCF_3SO_3-(EO)_6-(H_2O)_3$ (**8d**). Hydrogen atoms are omitted.

3.5. Classical Molecular Dynamics (MD) Simulations. The equilibrated configuration shows that the majority of H_2O molecules, Li^+, and the anion migrate from the hydrophobic ($C_9H_{19}-$ tail) to the hydrophilic domain. The microscopic structure is also illustrated by the radial distribution function (rdf) $g_{LiX}(r)$, as shown in Figure 9, which is defined as the ratio of the real number of atoms X located at a spherically symmetric distance r from Li to the ideal number that would exist if the microscopic fluid structure were perfectly homogeneous. In line with ab initio quantum chemistry calculations, Figure 9 qualitatively shows that the triflate oxygen, the water oxygen, the backbone nitrogen, and the ether oxygen atoms of PP could be found around Li^+ within 2−2.5 Å, indicating that a significant interaction exists between Li^+ and those atoms. From the integral of the first peak of $g_{LiX}(r)$ it can be found that each

TABLE 6: Averaged Distances (Å) from Li^+ to the Coordinated Oxygen, Nitrogen, and Ether Oxygen of PP (R_{Li-PP}), to the nearest Anion Oxygen (R_{Li-O-X}), and to the Water Oxygen (R_{Li-O-W}) in the Aggregates $XLi(H_2O)_{0-1}PP$ and Their Binding Energies (ΔE/kcal/mol), Enthalpies (ΔH), and Gibbs Free Energies (ΔG) of Formation at 298.2 K with HF/6-31G*

aggregates	structure	R_{Li-O-X}[c]	R_{Li-PP}[d]	R_{Li-O-W}	ΔE[a]	ΔE_0[b]	ΔH[b]	ΔG[b]
PP3−Li	**5b**		1.903(1)		−51.7	−48.3	−49.0	−40.6
PP3−Li	**5c**		1.962(2)		−75.7	−70.8	−71.6	−63.1
PP6−Li	**6b**		2.000(3)		−82.8			
PP6−Li	**6c**		1.984(3)		−131.5	−123.3	−124.4	−115.1
PP6−Li	**6d**		2.030(3)		−104.8	−96.2	−97.2	−86.4
PP6−Li	**6e**		2.063(4)		−95.5			
PP6−Li	**6f**		2.108(4)		−128.7	−116.2	−117.4	−110.4
PP6−LiX	**8a**	2.013(2)	2.063(2)		−37.1			
PP6−LiX	**8b**	2.053(2)	2.087(2)		−43.3	−41.9	−41.6	−27.5
PP6−LiX	**8c**	1.918(1)	2.083(3)		−59.1	−57.1	−57.0	−43.2
PP6−LiX−(H_2O)	**8d**	1.949(1)	2.196(2)	1.943	−65.4	−60.6	−61.3	−36.5

[a] For the complexes of Li^+ and PP3/PP6, $\Delta E = E(\text{complex}) - E(Li^+) - E(\text{PP})$, while for the binary and ternary aggregates containing CIP, $\Delta E = E(\text{aggregate}) - E(LiCF_3SO_3) - mE(H_2O) - E(\text{PP})$. [b] $\Delta E_0 = \Delta E + \text{ZPE}$; for comparison with Li−H_2O and Li−$(EO)_6$ systems BSSE values were included only for PP6−Li systems. [c] The number in parentheses refers to the coordination number of Li^+ with the triflate anion. [d] The number in parentheses refers to the coordination number of Li^+ with nitrogen and oxygen atoms of PP.

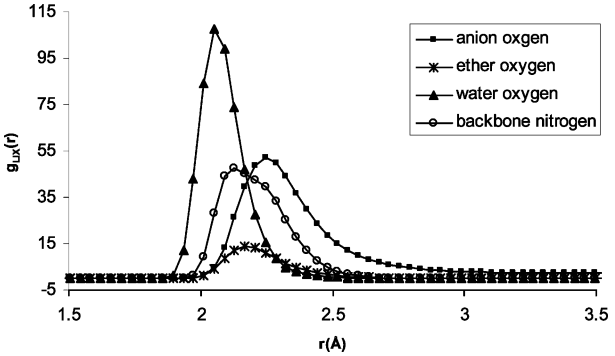

Figure 9. Radial distribution function g_{LiX} from molecular dynamics simulations for mixtures of PP (1), $LiCF_3SO_3$, and water at 300 K, illustrating distributions of the anion oxygen, ether oxygen, water oxygen, and backbone nitrogen atoms around Li^+ in the range of 1.5−3.5 Å.

Li^+ ion is complexed, on the average, with approximately 0.5 ether oxygen and 0.9 backbone nitrogen atoms, 1 water molecule, and 1.3 oxygen atoms from the triflate anion. The broad peak of g_{LiN} is an indication that Li^+ associates with more than one nitrogen atoms in certain complexes. A close inspection on the equilibrated configurations demonstrates that a considerable number of ion pairs are formed. Among them, two ion pairs could be clearly characterized to be a composite aggregate, Li^+ simultaneously interacting with nitrogen and ether oxygen atoms, and water molecules. Six ion pairs are surrounded only by one or two ether oxygen atoms and water, and one ion pair only by water. In addition, three Li^+ ions solvated by the ether oxygen and nitrogen atoms and by water molecules are also found. Overall, the microscopic solvation structure in the model PP polymer electrolyte exhibits a great variety of aggregates, such as "free" ions solvated by water and by ether oxygen and nitrogen atoms of PP, and solvated ion pairs. The calculated overall three-dimensional diffusion coefficients for Li^+, H_2O, and $CF_3SO_3^-$ estimated on the basis of the time evolution of their mean square displacements are 4.4×10^{-6}, 3.1×10^{-4}, and 2.2×10^{-5} cm^2/s, respectively.

4. Summary

The microscopic structure of a MEEP-like polyphosphazene electrolyte consisting of model PPs, $LiCF_3SO_3$, and water was investigated with ab initio quantum chemistry calculations and classical molecular dynamics simulations. The coordination of Li^+ with nitrogen atoms in the backbone, ether oxygens in the side chains, and water oxygen atoms was systematically studied. In general, nitrogen atoms have the strongest affinity for Li^+, while the ether oxygen and the water oxygen have comparable but smaller affinities for Li^+. Thus, the Li^+−N interaction is expected to significantly affect migration of Li^+ in these electrolytes. Li^+ is able to coordinate with multiple nitrogen atoms as well as with one or more ether oxygens. The pocket structures suggested by Luther,[11] where Li^+ coordinates with one nitrogen atom and its neighboring ether oxygen atoms, are not as stable as those where Li^+ coordinates with multiple (∼2−3) neighboring nitrogen atoms and one methoxy oxygen.

The calculated coordination pattern of Li^+ with $(EO)_6$ is consistent with the experimental result that Li^+ is most likely coordinated with five oxygen sites in crystalline salted PEO.[32,33] The structures found for the binary aggregate CIP−$(EO)_6$ and its analogue CIP−PP6/water, as well as for the ternary aggregate CIP−$(EO)_6$/PP6−water, were also consistent with experimental findings.[8] Their structures and thermodynamics indicate that the CIP is quite stable, and that its complete dissociation and transformation to less tight ion pairs, such as the solvent-shared ion pair, require higher degrees of solvation than those examined in calculations on the binary and ternary aggregates. Classical molecular dynamics simulations qualitatively reproduce the results of the quantum chemistry calculations. Considerable amounts of clustered ions are formed, in a variety of binary or

SCHEME 1: (A) High Li^+ Affinity Region Including N of the Backbone and Ether Oxygen of the Side Chain, (B) Low Li^+ Affinity Region Consisting of Ether Oxygen Atoms,[a] and and (C) Hydrophobic Region Made of a Carbon Matrix[b]

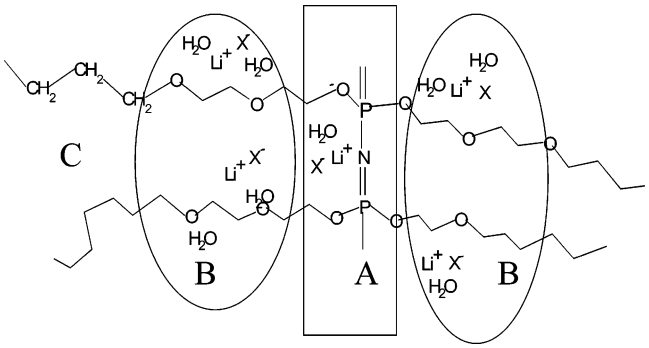

[a] Li^+ may jump among the side chains. [b]The high density of the region can prevent the penetration of H_2O.

ternary aggregates. Each Li^+ ion was found complexed, on the average, by approximately 0.5 ether oxygen atoms, 0.9 backbone nitrogen atoms, 1.0 water molecule, and 1.3 oxygen atoms from the triflate anion. On the basis of ab initio and MD simulations, the primary solvation structure can be described by Scheme 1, where Li^+ ions, either "free" or forming aggregates, are distributed over the backbone region and over the poly(ethylene oxide) portion of the side chain.

Acknowledgment. This work is partially supported by the National Science Foundation, grant CTS-9876065. Discussions with Dr. Harry Ploehn are gratefully acknowledged. Supercomputer resources provided by the National Center for Supercomputer Applications under grant CHE300055N are greatly appreciated.

References and Notes

(1) Allcock, H. A.; Kellam, I. E. C. The synthesis and applications of novel aryloxy/oligoethyleneoxy substituted polyphosphazenes as solid polymer electrolytes. *Soild State Ionics* **2003**, *156*, 401−414.

(2) Blonsky, P. M.; Shriver, D. F.; Austin, P.; Allcock, H. R. Polyphosphazene solid electrolytes. *J. Am. Chem. Soc*. **1984**, *106* (22), 6854−6855.

(3) Chang, Y.; Powell, E. S.; Allcock, H. R.; Park, S. M.; Kim, C. Thermosensitive Behavior of Poly(ethylene oxide)-Poly[bis(methoxyethoxyethoxy)-phosphazene] Block Copolymers. *Macromolecules* **2003**, *36* (7), 2568−2570.

(4) Littauer, E. L.; Tsai, K. C.; Hollandsworth, R. P. *J. Electrochem. Soc*. **1978**, *125*, 845.

(5) Urquidi-Macdonald, M.; Castaneda, H.; Cannon, A. M. Lithium fuel cells: I. Lithium/poly(organophosphazene) membrane anodes in KOH and seawater. *Electrochim. Acta* **2002**, *47* (15), 2495−2503.

(6) Lonergan, M. C.; Shriver, D. F.; Ratner, M. A. Polymer Electrolytes: The Importance of Ion-Ion Interactions in Diffusion Dominated Behavior. *Electrochim. Acta* **1995**, *40* (13−14), 2041−2048.

(7) Bruce, P. G. Structure and Electrochemistry of Polymer Electrolytes. *Electrochim. Acta* **1995**, *40* (13−14), 2077−2086.

(8) Rhodes, C. P.; Frech, R. Cation-anion and cation-polymer interactions in $(PEO)_nNaCF_3SO_3$ ($n = 1-80$). *Solid State Ionics* **1999**, *121*, 91−99.

(9) Sutjianto, A.; Curtiss, L. A. Li^+-Diglyme Complexes: Barriers to Lithium Cation Migration. *J. Phys. Chem. A* **1998**, *102* (6), 968−974.

(10) Baboul, A. G.; Redfern, P. C.; Sutjianto, A.; Curtiss, L. A. Li^+-$(Diglyme)_2$ and $LiClO_4$-Diglyme Complexes: Barriers to Lithium Ion Migration. *J. Am. Chem. Soc.* **1999**, *121* (31), 7220−7227.

(11) Luther, T. A.; Stewart, F. F.; Budzien, J. L.; LaViolette, R. A.; Bauer, W. F.; Harrup, M. K.; Allen, C. W.; Elayan, A. On the Mechanism of Ion Transport through Polyphosphazene Solid Polymer Electrolytes: NMR, IR, and Raman Spectroscopic Studies and Computational Analysis of ^{15}N-Labeled Polyphosphazenes. *J. Phys. Chem. B* **2003**, *107* (14), 3168−3176.

(12) Allcock, H. R.; Napierala, M. E.; Olmeijer, D. L.; Best, S. A.; Merz, K. M., Jr. Ionic Conduction in Polyphosphazene Solids and Gels: ^{13}C, 31P, and ^{15}N NMR Spectroscopy and Molecular Dynamics Simulations. *Macromolecules* **1999**, *32* (3), 732−741.

(13) Johansson, P.; Jacobsson, P. Ion Pairs in Polymer Electrolytes Revisited: An Ab Initio Study. *J. Phys. Chem. A* **2001**, *105* (37), 8504−8509.

(14) Merrill, G. N.; Webb, S. P.; Bivin, D. R. Formation of Alkali Metal/Alkaline Earth Cation water clusters, $M(H_2O)_{1-6}$, $M = Li^+$, Na^+, K^+, Mg^{2+}, and Ca^{2+}: An effective fragment potential (EFP) case study. *J. Phys. Chem. A* **2003**, *107*, 386-396.

(15) Redfern, P. C.; Curtiss, L. A. Quantum chemical studies of Li^+ cation binding to polyalkyloxides. *J. Power Sources* **2002**, *110* (2), 401−405.

(16) Becke, A. D. A new mixing of Hartree−Fock and local density-functional theories. *J. Chem. Phys.* **1993**, *98*, 1372−1377.

(17) Burke, K.; Perdew, J. P.; Wang, Y. *Electronic Density Functional Theory: Recent Progress and New Directions*; Dobson, J. F., Vignale, G., Das, M. P., Eds.; Plenum: New York, 1998.

(18) Breneman, C. M.; Wiberg, K. B. Determining atom-centered monopoles from molecular electrostatic potentials. The need for high sampling density in formamide conformational analysis. *J. Comput. Chem.* **1990**, *11*, 361.

(19) Boys, S. F.; Bernardi, F. *Mol. Phys.* **1970**, *19*, 553.

(20)] Barone, V.; Cossi, M. Quantum Calculation of Molecular Energies and Energy Gradients in Solution by a Conductor Solvent Model. *J. Phys. Chem. A* **1998**, *102*, 1995−2001.

(21) Cossi, M.; Rega, N.; Scalmani, G.; Barone, V. Energies, structures, and electronic properties of molecules in solution with the C-PCM solvation model. *J. Comput. Chem.* **2003**, *24* (6), 669−681.

(22) Wang, Y. X.; Nakamura, S.; Ue, M.; Balbuena, P. B. Theoretical studies to understand surface chemistry on carbon anodes for lithium-ion batteries: Reduction mechanisms of ethylene carbonate. *J. Am. Chem. Soc*. **2001**, *123* (47), 11708−11718.

(23) Frisch, M. J.; Trucks, G. W.; Schlegel, H. B.; Scuseria, G. E.; Robb, M. A.; Cheeseman, J. R.; Montgomery, J. A., Jr.; Vreven, T.; Kudin, K. N.; Burant, J. C.; Millam, J. M.; Iyengar, S. S.; Tomasi, J.; Barone, V.; Mennucci, B.; Cossi, M.; Scalmani, G.; Rega, N.; Petersson, G. A.; Nakatsuji, H.; Hada, M.; Ehara, M.; Toyota, K.; Fukuda, R.; Hasegawa, J.; Ishida, M.; Nakajima, T.; Honda, Y.; Kitao, O.; Nakai, H.; Klene, M.; Li, X.; Knox, J. E.; Hratchian, H. P.; Cross, J. B.; Adamo, C.; Jaramillo, J.; Gomperts, R.; Stratmann, R. E.; Yazyev, O.; Austin, A. J.; Cammi, R.; Pomelli, C.; Ochterski, J. W.; Ayala, P. Y.; Morokuma, K.; Voth, G. A.; Salvador, P.; Dannenberg, J. J.; Zakrzewski, V. G.; Dapprich, S.; Daniels, A. D.; Strain, M. C.; Farkas, O.; Malick, D. K.; Rabuck, A. D.; Raghavachari, K.; Foresman, J. B.; Ortiz, J. V.; Cui, Q.; Baboul, A. G.; Clifford, S.; Cioslowski, J.; Stefanov, B. B.; Liu, G.; Liashenko, A.; Piskorz, P.; Komaromi, I.; Martin, R. L.; Fox, D. J.; Keith, T.; Al-Laham, M. A.; Peng, C. Y.; Nanayakkara, A.; Challacombe, M.; Gill, P. M. W.; Johnson, B.; Chen, W.; Wong, M. W.; Gonzalez, C.; Pople, J. A. *Gaussian 03*, Revision A.1; Gaussian, Inc.: Pittsburgh, PA, 2003.

(24) Smith, W.; Forester, T. R. *DL_POLY*, Version 2.14; Daresbury Laboratory: Daresbury, 2003.

(25) Evans, D. J. Computer "experiment" for nonlinear thermodynamics of Couette flow. *J. Chem. Phys.* **1983**, *78* (6), 3297.

(26) Mayo, S. L.; Olafson, B. D.; W. A. Goddard, I. DREIDING: A Generic Force Field fo Molecular Simulations. *J. Am. Chem. Soc*. **1990**, *94* (26), 8897−8898.

(27) Berendsen, H. J. C.; Grigera, J. R.; Straatsma, T. P. The missing term in effective pair potentials. *J. Phys. Chem.* **1987**, *91*, 6269−71.

(28) Peng, Z.; Ewig, C. S.; Hwang, M.-J.; Waldman, M.; Hagler, A. T. Derivation of Class II Force Fields. 4. van der Waals parameters of alkali metal cations and halide anions. *J. Phys. Chem. A* **1997**, *101*, 7243−7252.

(29) Dzidic, I.; Kebarle, P. *J. Phys. Chem.* **1970**, *74*, 1466.

(30) Zhang, Y.; Pan, W.; Yang, W. Describing van der Waals Interaction in diatomic molecules with generalized gradient approximations: The role of the exchange functional. *J. Chem. Phys.* **1997**, *107*, 7921.

(31) Perdew, J. P.; Burke, K.; Ernzerhof, M. Generalized gradient approximation made simple. *Phys. Rev. Lett.* **1997**, *78* (7), 1396−1396.

(32) Gadjourova, Z.; Andreev, Y. G.; Tunstall, D. P.; Bruce, P. G. Ionic conductivity in crystalline polymer electrolytes. *Nature* **2001**, *412* (6846), 520−523.

(33) Gadjourova, Z.; Martin D.; Andersen, K. H.; Andreev, Y, G.; Bruce, P. G. Structures of the Polymer Electrolyte Complexes PEO_6:$LiXF_6$ (X = P, Sb), Determined from Neutron Powder Diffraction Data. *Chem. Mater*. **2001**, *13* (4), 1282−1285.

(34) Müller-Plathe, F.; van Gunsteren, W. F. Computer Simulation of a Polymer Electrolyte: Lithium Iodide in Amorphous Poly(ethylene oxide). *J. Chem. Phys.* **1995**, *103* (11), 4745−4756.

(35) Johansson, P.; Tegenfeldt, J.; Lindgren, J. Modelling amorphous lithium salt-PEO polymer electrolytes: ab initio calculations of lithium ion-tetra-, penta- and hexaglyme complexes. *Polymer* **1999**, *40* (15), 4399−4406.

(36) Szalewicz, K.; Cole, S. J.; Kolos, W.; Bartlett, R. J. A theoretical study of the water dimer interaction. *J. Chem. Phys*. **1988**, *89* (6), 3662−3673.

(37) Feller, D. Application of systematic sequences of wave functions to the water dimer. *J. Chem. Phys*. **1990**, *96* (8), 6104−6114.

(38) Curtiss, L. A.; Frurip, D. J.; Blander, M. Studies of molecular association in water and heavy water vapors by measurement of thermal conductivity. *J. Chem. Phys.* **1979**, *71* (6), 2703−11.

(39) Mao, G.; Saboungi, M.-L.; Price, D. L.; Badyal, Y. S.; Fischer, H. E. Lithium environment in PEO−$LiClO_4$ polymer electrolyte. *Europhys. Lett*. **2001**, *54* (3), 347−353.